FULL PAPER

Imaging the Electric Potential within Organic Solar Cells

Rebecca Saive, Michael Scherer, Christian Mueller, Dominik Daume, Janusz Schinke, Michael Kroeger, and Wolfgang Kowalsky*

The charge transport in organic solar cells is investigated by surface potential measurements via scanning Kelvin probe microscopy. Access to the solar cell's cross-section is gained by milling holes with a focused ion beam which enables the direct scan along the charge transport path. In a study of poly(3-hexylthiophene):1-(3-methoxycarbonyl)propyl-1-phenyl[6,6]C61 (P3HT:PCBM) bulk heterojunction solar cells, the open circuit voltage is built up at the top contact. A comparison of the potential distribution within normal and inverted solar cells under operation exhibits strongly different behaviors, which can be assigned to a difference in interface properties.

1. Introduction

Organic solar cells (OSCs) have gotten into the spotlight of scientific and industrial research, as they offer the possibility of inexpensive electrical power generation in versatile applications. There have been reports on maximum power conversion efficiencies of 10.0% for small molecule solar cells[1] and 8.6% for polymer solar cells.[2] The enhancement of solar cell performance is a constant interplay between the trial of new materials and device concepts on one hand and the systematic investigation of the underlying processes on the other. Many efforts have been undertaken to understand charge generation and charge separation in OSCs, for example by optical spectroscopy[3] or with scanning probe microscopy methods.[4] Fundamental concepts and timescales of these processes have been studied, but there are still many open questions especially concerning the generation of the photovoltage and subsequent charge transport. Charge transport studies in electronic devices have been performed by assessing the local surface potential with scanning Kelvin probe microscopy (SKPM), as demonstrated by several other groups.[5–7] This method is based on an atomic force microscopy (AFM) setup and thus restricted to measure at the sample's surface, whereas the charge transport in solar cells occurs vertically to the surface. For inorganic crystalline solar cells and light emitting devices, this problem was solved by cutting or cleaving the samples and measuring SKPM at the exposed cross-sections. The obtained results provide valuable information on the electrical properties of the devices.[8–10] In principle, it is also possible to cleave or cut organic solar cells and measure SKPM at the cross-section[11–12] but, because of the softness and non-crystallinity of the materials, these cross-sections are rough and smeared and it is hard to achieve sufficiently high energy resolution.[11] Therefore, we have developed a new method using a focused ion beam (FIB) to mill holes in solar cells and characterize the bare cross-section in-situ with SKPM. This method was demonstrated to be superior to above mentioned ex-situ techniques.[11] Here, we applied this novel technique to poly(3-hexylthiophene):1-(3-methoxycarbonyl) propyl-1-phenyl[6,6]C61 (P3HT:PCBM) bulk heterojunction (BHJ) solar cells in conventional and inverted device structures to analyze the origin of the open circuit voltage and to reveal charge transport barriers.

R. Saive, M. Scherer, C. Mueller, D. Daume, J. Schinke, Dr. M. Kroeger, Prof. W. Kowalsky
InnovationLab GmbH
Speyerer Str. 4, 69115 Heidelberg, Germany
E-mail: rebecca.saive@innovationlab.de
R. Saive, M. Scherer, J. Schinke, Dr. M. Kroeger, Prof. W. Kowalsky
TU Braunschweig
Institute for High-Frequency Technology
Schleinitzstr. 22, 38106 Braunschweig, Germany
R. Saive, M. Scherer, C. Mueller, D. Daume
University of Heidelberg
Kirchhoff-Institute for Physics
INF 227, 69120 Heidelberg, Germany

DOI: 10.1002/adfm.201301315

2. Results and Discussion

2.1. Surface Potential of Unbiased Cross-Section

First, we investigated the cross-section of a conventional BHJ solar cell with both contacts connected to ground potential. **Figure 1**a shows a scanning electron microscopy (SEM) image of the measured cross-section. It shows a bright contrast for the indium-tin oxide (ITO), a slightly darker contrast for the Al, and a dark contrast for the organic material. The SEM image was used to clearly identify the layers in the SKPM image which is shown in Figure 1b. In this measurement both contacts of the solar cell were grounded such that without illumination there was no net current flowing and the Fermi levels were aligned. Therefore, the signal reflects the local work function whereas one has to keep in mind that the displayed values are relative to the work function of the cantilever tip. Figure 1c shows a profile of the surface potential difference at the cross-section marked by the arrow in Figure 1b. The work function difference between ITO and Al is measured to be around 0.5 eV. For

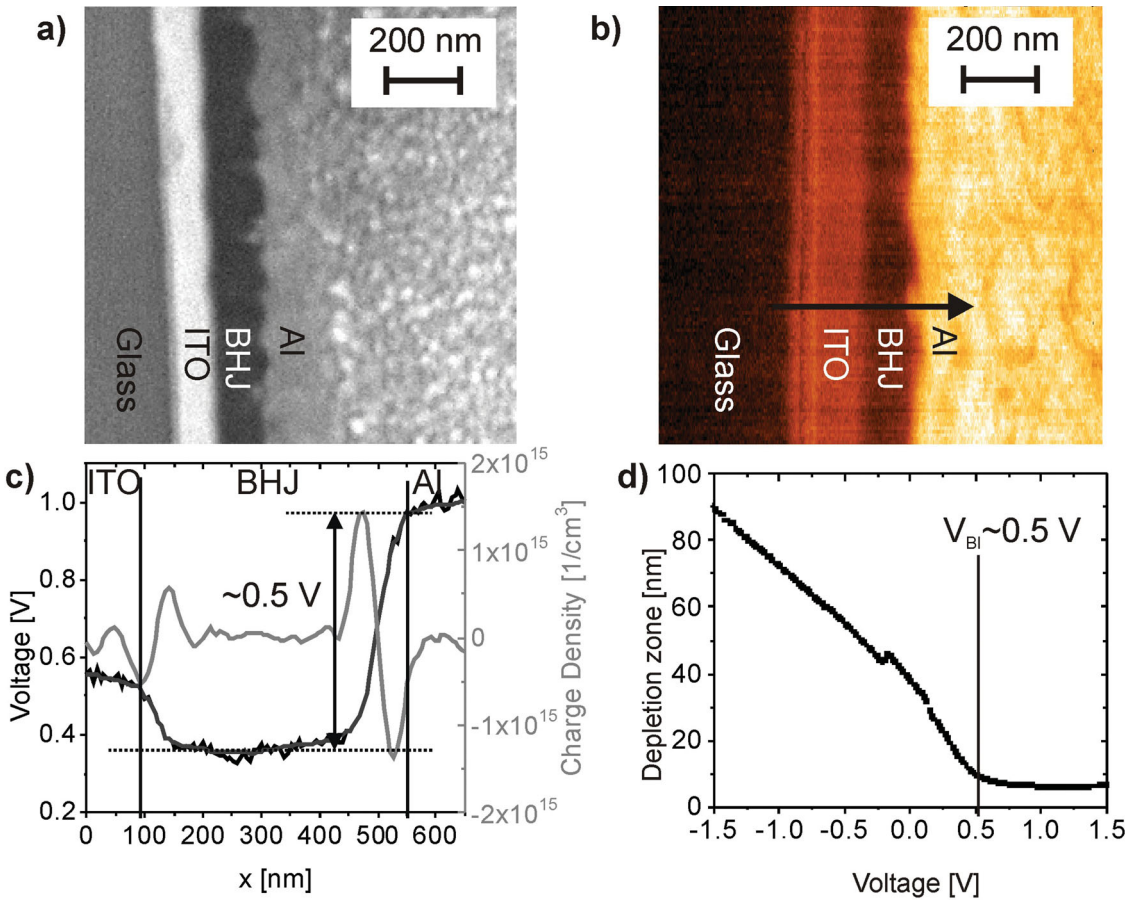

Figure 1. a) SEM image of the measured cross-section. It shows a bright contrast for the ITO, a slightly darker contrast for the Al and a dark contrast for the organic material. b) SKPM measurement of the cross-section with both contacts of the solar cell connected to ground. c) Black line: potential profile at the indicated arrow in (b). Dark gray line: smoothed signal. Bright gray line: derived charge carrier density. d) Depletion zone of the solar cell depending on the applied bias voltage derived from a *C–V* measurement.)

the BHJ, we measure a work function which is about 200 meV higher than that of ITO. From energy level measurements by photoelectron spectroscopy (XPS and UPS)[13,14] and from the measurements of Lee et al. with SKPM on a cleaved BHJ solar cell cross-section,[12] one would expect the BHJ's work function to be lower than the ITO's work function.[15] We performed our measurements several times on different devices and on cross-sections prepared by cleaving and microtome cutting[11] with the same results, so that we can be sure that this effect is not an artifact of the FIB milling. It might be caused by interface effects like Fermi level pinning or dipole generation. It is also possible that the bulk heterojunction in the device forms another Fermi level than the single materials. With our method, an entire explanation cannot be given and the behavior should be further studied for example by X-ray photoelectron spectroscopy (XPS) interface studies. However, it can be excluded that the effect is caused by the poly(3,4-ethylenedioxythiophene):poly-(styrenesulfonate) (PEDOT:PSS) layer, as the behavior for inverted solar cells without PEDOT:PSS is similar (compare profiles in Section 2.3).

On the same solar cell, we also performed capacitance-voltage (*C–V*) measurements with an impedance spectrometer. In a classical Schottky or p–n junction diode, the depletion zone acts as the dielectric of a plate capacitor. As the depletion zone decreases with increasing forward bias voltage, the capacitance increases with increasing voltage and becomes the highest when the applied voltage matches the built-in voltage. The width d of the depletion zone can be calculated by $d = \varepsilon\varepsilon_0 A/C$, where A is the active area of the sample and C the measured capacitance. The relative permittivity ε was approximated to 3.5. The depletion zone dependence on the applied voltage is shown in Figure 1d. It becomes minimal at a bias voltage of 0.5 V and therefore the built-in voltage of the diode can be deduced to be about 0.5 V. This is consistent with the open circuit voltage of the solar cell at one sun illumination. Furthermore, the value corresponds to the measured contact potential difference (CPD) of Al and ITO, which confirms the theory that this difference dictates an upper limit for the bulit-in voltage and, hence, the open circuit voltage.[16,17]

Furthermore, it is interesting to compare the derived width of the depletion zone from the macroscopic *C–V* measurement with the result from the microscopic SKPM measurement, as these are entirely complementary methods. From the *C–V* measurement we gain a width of 30–40 nm at 0 V bias voltage.

In the SKPM measurement, the decrease of the surface potential between the contacts and the BHJ should correspond to the depletion zone. This signal is smeared compared to the real potential distribution due to the interaction of the whole cantilever with the sample surface which limits the lateral resolution to 20 nm.[18] Therefore the width of 50–70 nm derived from the slope of the CPD profile in Figure 1c could be expected. Moreover, it is possible to derive the charge carrier density from the smoothed potential drop (marked by the dark gray line in Figure 1c) by the Poisson equation

$$\Delta\Phi = \varrho(r)/\varepsilon\varepsilon_0 \quad (1)$$

Hereby, we can estimate a carrier concentration of about 10^{15} cm^{-3}. The derived spatial charge distribution is shown by the bright gray line in Figure 1c. From the *C–V* measurement, the charge carrier density can be derived by the Schottky-model[19] to 10^{16}–10^{17} cm^{-3}. The lower value deduced from the SKPM data likely arises from the limited lateral resolution, or from the fact that the Schottky-model overestimates the carrier concentration in organic semiconductors as it does not include disorder effects.

2.2. Open-Circuit Voltage

A crucial issue in the understanding of the charge generation process is the origin of the open-circuit voltage. Therefore, in the next experiment, we measured the surface potential along a conventional BHJ solar cell cross-section with and without illumination and unplugged the connections towards the OSC electrodes to create open circuit conditions and so be able to investigate the region of the open circuit voltage generation. In **Figure 2**a, the described experiment is demonstrated. The SKPM signal was recorded in horizontal scan lines according to the tip movement along the edge, starting at the bottom of the graph. The sample conditions were altered during measurement.

Thus, in one image one finds data for several different sample conditions, for example, in dark or illuminated, or a change in which device electrode was contacted to ground. For each sample condition, several line scans were taken and the switch from one sample condition to another was manually performed between two line scans.

In region A, one can observe the potential distribution for the non-illuminated, zero-bias case, which is equivalent to the driving conditions of the device in Figure 1. If one now turned on the light, but kept the device in short circuit condition (region B), the potential distribution would remain unchanged, as both contacts would be forced to equal potential.

In region C, we unplugged the ITO contact, and one can observe that the signal at the ITO contact shifted to a higher value. In region D, we replugged the ITO contact again, which therefore instantly shifted back to the original value. In region E, the Al contact was taken off and the signal on this contact shifted downward. It returned to its original value when we turned the illumination off (region F). Figure 2b shows profiles of the CPD in region B and C and Figure 2c shows profiles in region E and F. Note that the layer thickness of the BHJ was not constant throughout the whole sample area which leads to slightly different shapes of the potential profiles. Nevertheless, one can estimate the shift of the potential on the contacts in both cases being around 200 mV. As already mentioned above, it was not possible to illuminate the solar cell at high intensity during measurement because of heating issues. Therefore a reduced open circuit voltage of 200 mV could only be built up as was also confirmed by *I–V* measurements (**Figure 3**d). To further investigate the position of the main voltage drop, relative spectra were calculated. That means, we use the 0 V profile (which corresponds to the relative work function) as a base line to which all other profiles are referred by subtraction of the base line profile. These work function corrected profiles are shown in Figure 2d,e, respectively. Based on these profiles, we can state that the drop of the open circuit voltage mainly occurs at the interface between Al and the BHJ, no matter which contact was plugged off.

In summary, the results show that our measurement method offers the possibility to understand macroscopic properties like the built-in and the open circuit voltage by microscopic studies of the material interfaces.

2.3. Surface Potential Under Bias Voltage

One of the most important issues in improving solar cells is the transport and the release of the photo generated charge carriers. Contacts have to be optimized in such a way that they hinder the charge transport as little as possible. With our method, it is possible to directly study the contact interfaces and to identify barriers for the charge transport. By characterizing the cross-section at different bias voltages, we can map the potential distribution under operation. A work function correction of the data relative to the 0 V base line, as described above, leads to relative spectra which contain only the effect of the applied voltage and can therefore indicate transport barriers by high potential drops. **Figure 4** shows the results of such a study. At each applied voltage we measured a scan field of 2×0.75 μm^2 and took a profile in each image at the same position. In Figure 4a, the profiles of the surface potential in a conventional BHJ solar cell at bias voltages between −2 V and +1.5 V are shown. Figure 4b shows the profiles for an inverted BHJ solar cell in the range between −0.5 V and 2 V. For both cell types, the measurements with bias voltages in backward direction were unproblematic and we chose to apply up to 2 V backward voltages respectively. In forward direction, we observed a measurement drift because of Joule heating and were therefore restricted to measurements up to +1.5 V for conventional and up to −0.5 V for inverted solar cells as the current in forward direction was higher in the inverted cells (compare Figure 3c,d). Figure 4c,d illustrate the respective relative potential distributions.

In Figure 4c, it becomes visible that in the conventional BHJ solar cell the applied voltage mainly drops at the interface between each contact and the BHJ approximately to the same amount and that there is nearly no drop of potential within the BHJ. However, in the inverted solar cell, the potential drop occurs exclusively in the BHJ and there is no dip on the contacts as can be seen in Figure 4c. Note that this effect is highly reproducible and could be observed for many individual solar cells.

This varying behavior can be explained by different conditions at the interfaces caused by two main effects. First,

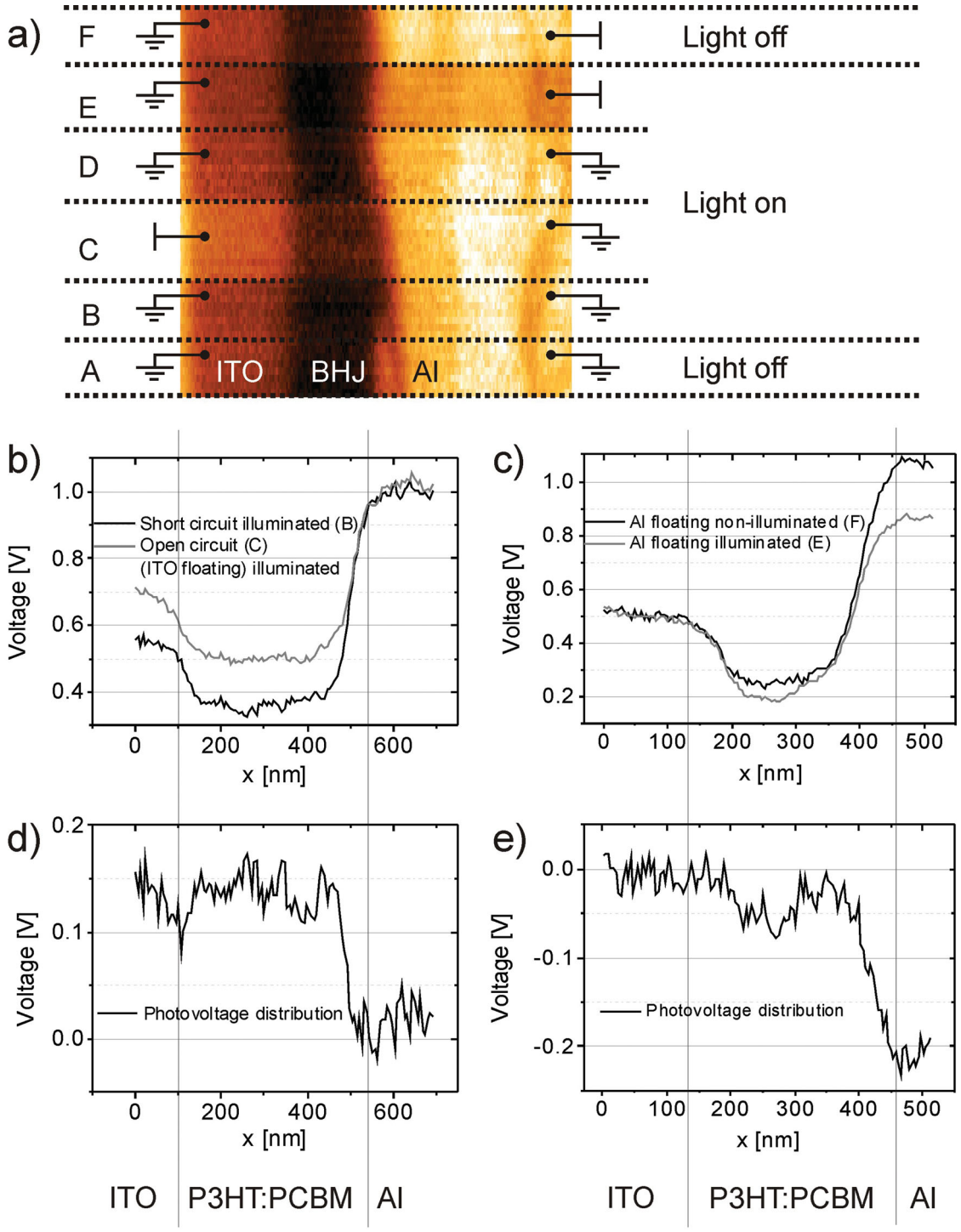

Figure 2. a) SKPM image of the OSC cross-section under varying conditions. b) Profiles through regions B and C and c) to the regions E and F. d,e) Relative potential distributions of (b) and (c).

the injection barriers from the BHJ to the contact materials can differ for the conventional and the inverted solar cells. P3HT:PCBM BHJs are known for the enrichment of one specie on the top and on the bottom respectively depending on the substrate properties. This demixture is reminiscent of the spinodal decomposition of material blends and has been studied by simulations as well as by experiments.[20,21] Usually the P3HT enriches at the top of the BHJ which is beneficial for inverted structures.[22] This selective segregation depends on the surface energy of the bottom contact.[23] The surface energy can be altered by an interfacial dipole layer,[24,25] which in this case is formed by the polyethylenimine ethoxylated (PEIE).[26,27]

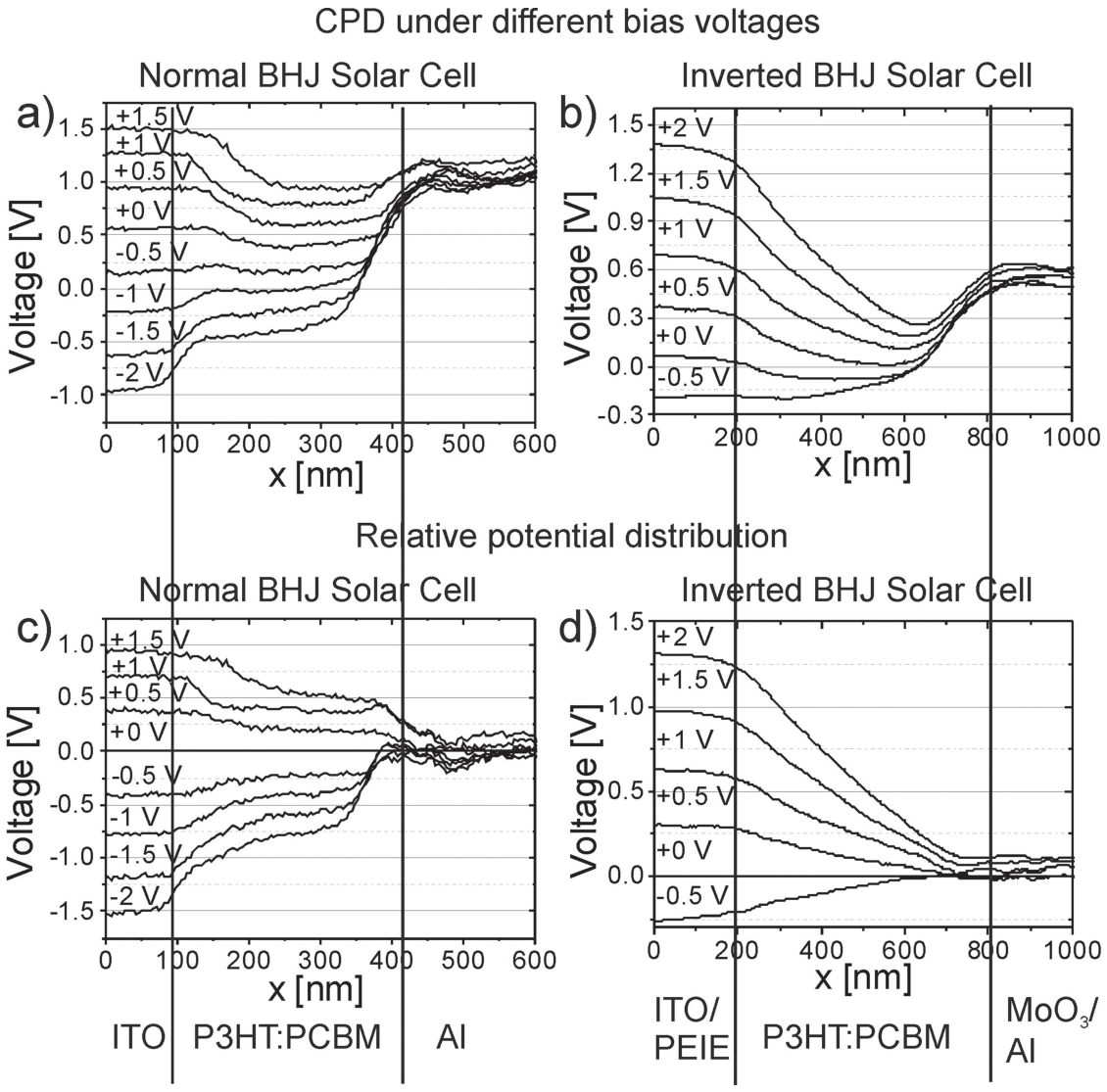

Figure 3. Profiles of the surface potential of a) a conventional BHJ solar cell at bias voltages between –2 V and 1.5 V and b) an inverted BHJ solar cell at bias voltages between –0.5 V and 2 V. c,d) Respective relative potential distributions.

Additionally, polymers like PEIE are known to lower injection barriers,[26,27] such that an enhanced injection compared to the conventional OSC is likely. Summarizing, a likely explanation for the different potential distributions are smaller injection barriers in the inverted than in the conventional OSCs. Figure 3c,d shows that the current in the inverted cell is higher than in the conventional cell which is consistent with this explanation. Note that the *J–V* curves shown in Figure 3 belong to the very same solar cells as the data in Figure 4. One might also think of a second explanation: the observed potential distribution in conventional BHJ solar cells can be explained by the above described morphology property, which cannot be spatially resolved by the SKPM as of its small structure size of a few nanometers. If there was an enrichment of single species at the top and at the bottom contact, then a potential drop at the contact would be measured even if the real drop occurs between the P3HT and the PCBM.

We will investigate this open question by imaging the morphology with a transmission electron microscope (TEM) and by performing measurements on bilayer devices.

3. Conclusions

We could show that in situ SKPM measurements on FIB milled cross-sections of organic solar cells offer the possibility to directly observe their potential distribution. Thereby, macroscopic characteristics of the solar cells were understood by microscopic measurement results. In a P3HT:PCBM BHJ solar cell, the open circuit voltage dropped at the top contact. If a voltage was applied to a conventional BHJ OSC, the potential dropped at the contacts, whereas in an inverted solar cell the potential dropped along the BHJ. As further steps, we plan to apply our measurement technique to bilayer P3HT:PCBM

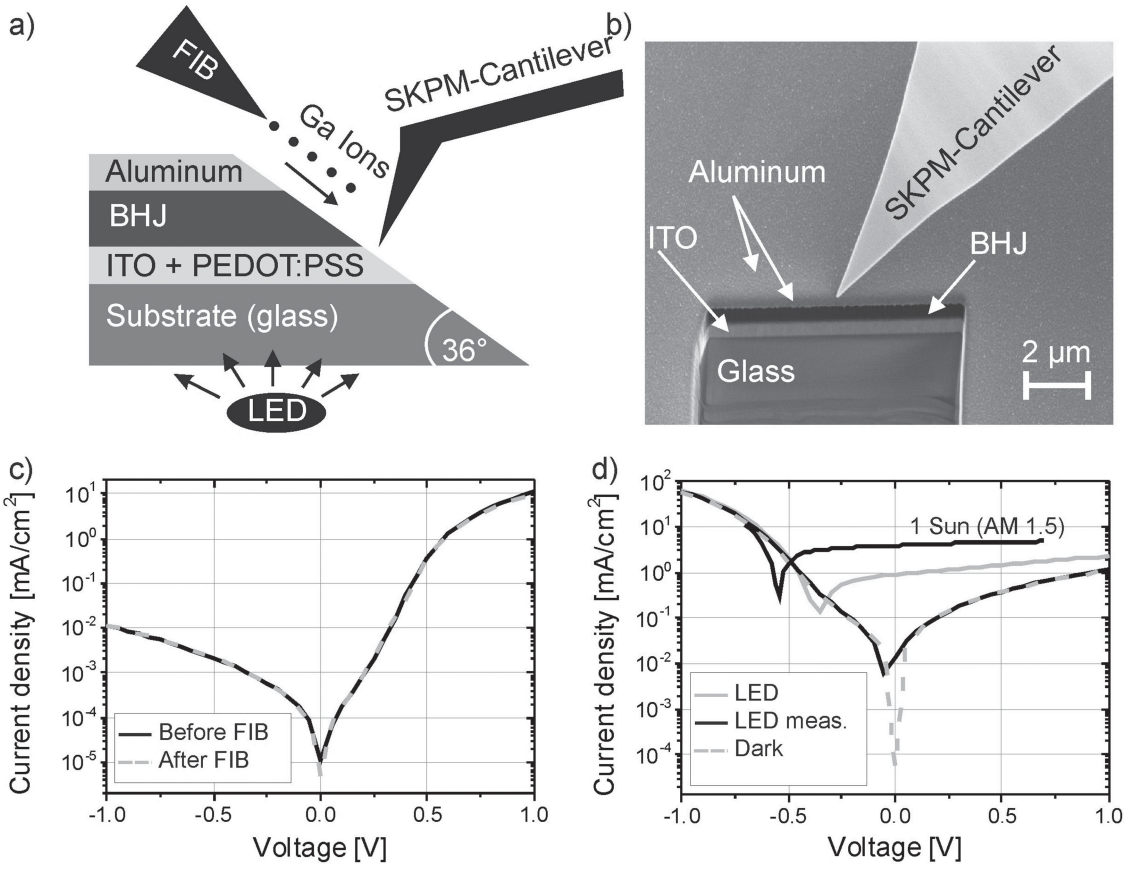

Figure 4. a) Schematic visualization of the sample characterization procedure. A small hole is milled into the solar cell by means of a FIB and afterwards the exposed cross-section is characterized with scanning probe microscope (SPM) in dark or by illumination via a light-emitting diode (LED). b) SEM image of a cantilever tip scanning the cross-section of a BHJ solar cell. c) *J–V* curve of a conventional BHJ solar cell before and after FIB milling. d) *J–V* curve of an inverted solar under 1 sun illumination, under LED illumination in the measurement setup (LED), under LED illumination in the setup during SKPM measurements (LED meas.) and in the dark.

solar cells and to correlate the measurements with morphology investigations by TEM.

4. Experimental Section

BHJ solar cells were fabricated on ITO-coated glass that had been patterned by photolithography to achieve a defined contact structure. The substrate size was chosen to be 5 mm × 5 mm as this is the maximum sample size which can be handled within our analytical setup. An approximately 25 nm thick PEDOT:PSS buffer layer was spin coated on top of the ITO electrode. To prepare active layers of P3HT:PCBM blends, P3HT, and PCBM were dissolved in chlorobenzene in a weight ratio of 1:1 with a total concentration of 20 mg mL^{-1} for each material. The solution was spin coated onto the PEDOT:PSS coated substrate at a speed of 2000 rpm. As the substrate size was rather small, the resulting layers became inhomogeneous with thicknesses of 2–3 µm at the edge of the substrate and about 200 nm at its center. As top electrode, 6 Å LiF and 100 nm Al were thermally evaporated. For the fabrication of the inverted solar cells, PEIE[28] was spin coated on top of the patterned ITO substrate. PEIE served as work-function-lowering agent and ITO became the bottom cathode in the inverted OPV architecture. The BHJ was deposited as in the case of the non-inverted solar cells. A 10 nm layer of MoO_3 with 100 nm of Al on top served as the top anode contact. The samples have been prepared under nitrogen atmosphere. They came into contact with ambient air for a few minutes during transport to vacuum. Possible influences of oxygen doping on the potential distribution have been investigated by Morris et al.[29] Immediately after their preparation, the solar cells were characterized under illuminated (AM 1.5) conditions. They exhibit an open-circuit voltage of 0.55 V and a short-circuit current of about 8 mA cm^{-2} with a maximum fill factor of 70%. The results for normal and inverted solar cells were similar. For determination of the local surface potential a combined system of a Carl Zeiss crossbeam microscope and a DME scanning probe microscope (SPM) was used. The crossbeam microscope contains a SEM and a FIB which can be used for imaging as well as for controlled material ablation in the nano- to micrometer range. 8 µm × 8 µm holes with a depth of about 2 µm were milled into the solar cells with the FIB at an acceleration voltage of 30 kV and an ion current of 500 pA. The integrated SPM allowed for an in situ measurement of the exposed cross-section with AFM and SKPM, whereas the SEM was used to position the cantilever tip on the microscopic cross-section. Figure 3a schematically shows the described process and Figure 3b shows a SEM image of a cantilever tip scanning the cross-section of a BHJ solar cell.

SKPM is a SPM method that determines the CPD between the tip of the cantilever and the sample surface.[30] The CPD is a superposition of the work function difference and the applied voltage. Without an applied voltage a material with high work function shows a lower SKPM signal than a material with lower work function. To gain information about the bias-induced voltage distribution, the CPD at 0 V bias voltage (which corresponds to the relative work function) has to be subtracted

from the signal under bias voltage. We used Pt/Ir coated cantilever tips and performed one-pass amplitude modulated (AM) SKPM such that topography and surface potential were measured simultaneously with a spatial resolution (of the surface potential) of about 20 nm and an electronic resolution of about 10 mV.[31] We excited the tip with a 4 V AC signal and scanned with a velocity of 0.25 μm s^{-1} to provide maximum resolution in vacuum. To enable the characterization of an operating device, the solar cell has to be contacted and illuminated within the microscope. Sample illumination was provided by an inorganic light-emitting diode (LED), which was fixed on the sample holder beneath the solar cell. This method led to non-standard (AM 1.5) illumination of the solar cell. Furthermore, the LED could not be operated at high power as the heat dissipation in the vacuum system is poor and the SPM measurement starts drifting or is not possible at all because of the heating at too large LED power. Figure 3d shows *J–V* curves of an inverted solar cell under AM 1.5 illumination (upper black curve), under illumination with the LED at maximum power (gray curve), under LED illumination during the measurement (lower black curve) and in the dark (dashed gray curve). A crucial point of the method is the question to what extend the solar cell is influenced by FIB milling. A comparison of current voltage characteristics captured before and after the FIB treatment (Figure 3c) shows that there is no influence of the FIB in, at least, the macroscopic characteristics of the solar cell. Nevertheless, as the milled hole represents only a small fraction of the active area a slight local variation of conductivity would probably not affect the *J–V* curves. Particularly, as we could observe strong doping capabilities of the FIB on 6,13-bis(triisopropylsilylethynyl)-pentacene (TIPS-pentacene),[32] we also investigated the same solar cells with cross-sections prepared by cleaving and microtome cutting, respectively.[11] Those samples show qualitatively very similar behavior which can be judged as confirmation for the FIB having no significant influence on the presented SKPM results.

Acknowledgements

The authors acknowledge the German Federal Ministry of Education and Research (BMBF) for generous financial support (FKZ 13N10794, FKZ 13N10723).

Received: April 18, 2013
Revised: May 14, 2013
Published online: June 19, 2013

[1] M. A. Green, K. Emery, Y. Hishikawa, W. Warta, E. D. Dunlop, *Prog. Photovoltaics: Res. Appl.* **2012**, *20*, 12.
[2] L. Dou, J. You, J. Yang, C.-C. Chen, Y. He, S. Murase, T. Moriarty, K. Emery, G. Li, Y. Yang, *Nat. Photonics* **2012**, *6*, 180.
[3] I. A. Howard, F. Laquai, *Macromol. Chem. Phys.* **2010**, *211*, 2063.
[4] L. S. C. Pingree, O. G. Reid, D. S. Ginger, *Adv. Mater.* **2009**, *21*, 19.
[5] E. C. P. Smits, S. G. J. Mathijssen, M. Cölle, A. J. G. Mank, P. A. Bobbert, P. W. M. Blom, B. de Boer, D. M. de Leeuw, *Phys. Rev. B* **2007**, *76*, 125202.
[6] K. P. Puntambekar, P. V. Pesavento, C. D. Frisbie, *Appl. Phys. Lett.* **2003**, *83*, 5539.
[7] L. C. Teague, B. H. Hamadani, O. D. Jurchescu, S. Subramanian, J. E. Anthony, T. N. Jackson, C. A. Richter, D. J. Gundlach, J. G. Kushmerick, *Adv. Mater.* **2008**, *20*, 4513.
[8] C.-S. Jiang, H. R. Moutinho, D. J. Friedman, J. F. Geisz, M. M. Al-Jassim, *J. Appl. Phys.* **2003**, *93*, 10035.
[9] T. Glatzel, H. Steigert, S. Sadewasser, R. Klenk, M. Lux-Steiner, *Thin Solid Films* **2005**, *480*, 177.
[10] R. Shikler, T. Meoded, N. Fried, Y. Rosenwaks, *Appl. Phys. Lett.* **1999**, *74*, 2972.
[11] M. Scherer, R. Saive, D. Daume, M. Kröger, W. Kowalsky, *Sample preparation for scanning Kelvin probe microscopy studies on cross sections of organic solar cells*, unpublished.
[12] J. Lee, J. Kong, H. Kim, S.-O. Kang, K. Lee, *Appl. Phys. Lett.* **2011**, *99*, 243301.
[13] Z.-L. Guan, J. B. Kim, H. Wang, C. Jaye, D. A. Fischer, Y.-L. Loo, A. Kahn, *Org. Electron.* **2010**, *11*, 1779.
[14] Z. Xu, L.-M. Chen, M.-H. Chen, G. Li, Y. Yang, *Appl. Phys. Lett.* **2009**, *95*, 013301.
[15] Y. Park, V. Choong, Y. Gao, B. R. Hsieh, C. W. Tang, *Appl. Phys. Lett.* **1996**, *68*, 2699.
[16] C. J. Brabec, A. Cravino, D. Meissner, N. S. Sariciftci, T. Fromherz, M. T. Rispens, L. Sanchez, J. C. Hummelen, *Adv. Funct. Mater.* **2001**, *11*, 374.
[17] V. D. Mihailetchi, P. W. M. Blom, J. C. Hummelen, M. T. Rispens, *J. Appl. Phys.* **2003**, *94*, 6849.
[18] D. S. H. Charrier, M. Kemerink, B. E. Smalbrugge, T. de Vries, R. A. J. Janssen, *ACS Nano* **2008**, *2*, 622.
[19] W. Schottky, *Z. Phys.* **1942**, *118,* 539.
[20] K. Binder, *Acta Polymer.* **1995**, *46*, 204.
[21] C. McNeill, *Energy Environ. Sci.* **2012**, *5*, 5653.
[22] Z. Xu, L.-M. Chen, G. Yang, C.-H. Huang, J. Hou, Y. Wu, G. Li, C.-S. Hsu, Y. Yang, *Adv. Funct. Mater.* **2009**, *19*, 1227.
[23] D. S. Germack, C. K. Chan, R. J. Kline, D. A. Fischer, D. J. Gundlach, M. F. Toney, L. J. Richter, D. M. De Longchamp, *Macromolecules* **2010**, *43*, 3828.
[24] S. A. Paniagua, P. J. Hotchkiss, S. C. Jones, S. R. Marder, A. Mudalige, F. S. Marrikar, J. E. Pemberton, N. R. Armstrong, *J. Phys. Chem. C* **2008**, *112*, 7809.
[25] P. E. Laibinis, G. M. Whitesides, *J. Am. Chem. Soc.* **1992**, *114*, 1990.
[26] J. W. Shim, H. Cheun, J. Meyer, C. Fuentes-Hernandez, A. Dindar, Y. Zhou, D. K. Hwang, A. Kahn, B. Kippelen, *Appl. Phys. Lett.* **2012**, *101*, 073303.
[27] H. Kang, S. Hong, J. Lee, K. Lee, *Adv. Mater.* **2012**, *24*, 3005.
[28] Y. Zhou, C. Fuentes-Hernandez, J. Shim, J. Meyer, A. J. Giordano, H. Li, P. Winget, T. Papadopoulos, H. Cheun, J. Kim, M. Fenoll, A. Dindar, W. Haske, E. Najafabadi, T. M. Khan, H. Sojoudi, S. Barlow, S. Graham, J.-L. Brédas, S. R. Marder, A. Kahn, B. Kippelen, *Science* **2012**, *336*, 327.
[29] J. D. Morris, T. L. Atallah, C. J. Lombardo, H. Park, A. Dodabalapur, X.-Y. Zhu, *Appl. Phys. Lett.* **2013**, *102*, 033301.
[30] M. Nonnenmacher, M. P. O'Boyle, H. K. Wickramasinghe, *Appl. Phys. Lett.* **1991**, *58*, 2921.
[31] W. Melitz, J. Shen, A. C. Kummel, S. Lee, *Surf. Sci. Rep.* **2011**, *66*, 1.
[32] R. Saive, L. Mueller, E. Mankel, W. Kowalsky, M. Kroeger, *Org. Electron.* **2013**, *14*, 1570.